LUND UNIVERSITY
Faculty of Science

Site localisation on bacterial surface proteins using super-resolution imaging

Vibha Kumra

Thesis submitted for the degree of Master of Science
Project duration: 5 months

Supervised by Jason Beech[1], Pontus Nordenfelt[2] and Jonas Tegenfeldt[1]

Department of Physics
[1]Division of Solid State Physics [2]Division of Infection Medicine at BMC
May 2018

Populärvetenskaplig sammanfattning

I snart 500 år har människan använt sig av diverse optiska instrument för att betrakta sådant som inte är möjligt att se med blotta ögat. Teleskop har använts för att studera himlakroppar och mikroskop för att exempelvis undersöka små biologiska beståndsdelar.

Det finns idag många olika metoder inom optisk mikroskopi men samtliga följer en liknande grundprincip. Objektet som ska avbildas exponeras för någon typ av energikälla (oftast laserstrålning), interagerar med den inkommande energin och avger därmed förändrad strålning som detekteras av en apparat.

Till följd av fysikens lagar finns det en specifik begränsning på hur god upplösning man kan lyckas få med ett konventionellt optiskt intrument. Denna så kallade diffraktions-begränsning beskrevs och myntades av Ernst Abbe år 1873 och har länge därefter betraktats som oöverkomlig. De bästa konventionella mikroskop kan idag nå en upplösning på cirka 300 nanometer (0.0000003 meter). Detta är inte tillräckligt för att exempelvis undersöka proteininteraktioner. De senaste åren har det dock dykt upp innovativa och fascinerande tekniker som lyckas överkomma diffraktionsbarriären. Dessa tekniker kallas kollektivt för super-resolutionstekniker och två av de vanligaste är STED och STORM.

I denna studie är vi intresserade av att avbilda bakterier för att förstå hur deras ytstrukturer interagerar med våra kroppar. Mer specifikt vill vi kunna besvara följande fråga: var binder bakterierna till våra kroppsegna molekyler och hur påverkar det deras chans att överleva och göra oss sjuka? Detta projekt ämnar att undersöka huruvida super-resolutionsteknikerna STORM och STED kan vara användbara i syfte att lokalisera bindningsplatser på bakterier.

STED systemet har en ringformad laser runt den vanliga lasern i ett mikroskop med syftet att, paradoxalt nog, minimera det inkommande ljusets utbredning. Man kan se det som att den ringformade lasern hämmar normal ljusinteraktion vid utkanterna av den vanliga lasern. STED har visats kunna uppnå en upplösning på 30-80 nanometer.

STORM systemet använder sig av ”blinkande” molekyler som objektet ifråga märks med. Genom mätning av tusentals blinkningar kan man matematiskt rekonstruera en resulterande bild med i teorin oändlig upplösning. Denna begränsas därför enbart av de blinkande molekylernas storlek, vilken ligger runt 20-30 nanometer.

Det finns flera praktiska för- och nackdelar med STORM och STED. Generellt kräver STED mer avancerad teknisk hantering medan STORM beror starkt på hur de biologiska proverna förbereds. Projektet har involverarat en hel del optimering genom många olika försök. I denna studie fick vi hög bildkvalite med STED. Detaljrikedomen var markant högre i STED-bilderna jämfört med diffraktionsbegränsade tekniker och STORM. Vi tror att avbildning med STORM kräver ytterliggare optimering av metod och analys.

Efter avbildning är det möjligt att använda bildhanteringstekniker för att framhäva detalj och information som vi även har testat. I detta projekt undersöktes dessutom en statistisk metod för att kunna kvantifiera resultaten på bästa sätt. STED bilderna, tilsammans med vår statistiska metod, möjliggjorde bestämning av en inbindningsplats med precision på 3.6 nanometer.

Contents

Acronyms and Abbreviations

CCD Charged-Couple Device.

COT Cyclooctatetraene.

dSTORM direct Stochastic Reconstruction Optical Microscopy.

EM Electron Microscopy.

Fab Fragment antigen binding.

Fc Fragment crystallizable.

FWHM Full Width at Half Maximum.

IgG Immunoglobulin G.

PSF Point Spread Function.

SNR Signal-to-Noise Ratio.

STED Stimulated Emission Depletion.

STORM Stochastic Reconstruction Optical Microscopy.

TIRF Total Internal Reflection Fluorescence.

WGA Wheat Germ Agglutinin.

Abstract

Several significant pathogenic bacteria exhibit surface proteins that bind human antibodies, preventing them from being recognized by the human immune system. These bacteria are thus protected from elimination and can survive in the host organism. One common such bacteria is the *Streptococcus pyogenes* that exhibits the antibody binding M protein on its surface. *Streptococcus pyogenes* causes more than 700 million uncomplicated throat and skin infections annually and can be at root of rare but very serious invasive infections such as sepsis. Understanding the mechanism behind the binding tendencies of *Streptococcus pyogenes* may thus help explain what causes this significant difference in prevalence of infectious severity.

The aim of this study was to evaluate whether or not the super-resolution techniques stimulated emission depletion (STED) and stochastic optical reconstruction microscopy (STORM) are viable optical techniques for relative localization studies of bacteria-bound antibodies. Binding sites on bacterial surface proteins were localised using the IgGFc-binding site on M protein as its location was known beforehand. The bacterial membrane was adopted as a reference region.

The necessary resolution required for site localisation on M proteins was acquired by applying statistical methods based on particle averaging and deconvolution on high resolution images. STED and STORM images were taken of samples prepared and analysed in the same manner. The two super-resolution techniques were compared to one another in terms of image quality, practicality and more specifically for the use of site localisation on bacterial surface proteins.

The distance between the membrane and the binding site on the M protein was calculated with the STED images to be 43.5 ± 3.6 nm which may be a reasonable result according to previous data [1]. The mean distance in the STORM images was calculated to be 124.8 ± 134.3 nm suggesting that the STORM procedure may require more optimisation. Interestingly, even though the image quality was low in the confocal images, the mean distance determined with these was 43.5 ± 4.7nm which is a reasonable distance with a narrow confidence interval. Deconvolution did not seem to have a significant impact on any set of images. According to our results, STED together with a particle averaging method, may be an appropriate technique for relative site localisation studies on bacterial surface proteins. Our results also suggest that confocal microscopy together with an averaging method may be a reasonable alternative for relative site localisation.

1 Introduction

Bacteria have co-evolved alongside humans throughout their common existence. They have thereby developed very specific defence and target mechanisms against one another. The various biological processes and structures involved in host defence are collectively referred to as the immune system. The human immune system consists of many different mechanisms, several organs and a large variety of specialised cells and proteins. A functional human immune system can detect harmful microbes known as pathogens and eliminate them from the body [2].

The antibody is a protein that plays an important role in immunity. An antibody is a globular Y-shaped protein of approximately 150 kiloDaltons. (see Fig. 2 A) The primary purpose of the antibody is to recognize and bind to characteristic protein structures, called antigens, on harmful microorganisms. Antibodies therefore have variable regions that differ depending on what antigen they are designed to recognize. These regions are referred to as fragment antigen binding (Fab)

regions and are supposed to bind to the pathogen of interest, exposing the remaining fragment crystallizable (Fc) region on the microbial surface. The Fc-region can thereafter be detected by Fc-receptors on the surface of so called phagocytic cells. The pathogen can thus be engulfed and eradicated by these cells. Five different kinds of antibodies can be found in the human body. Immunoglobulin G (IgG) is the most abundant and plays the main role in clearance of bacteria via phagocytosis [3].

Several significant pathogenic bacteria express surface proteins with antiphagocytic IgGFc-binding sites [4] [5] [6] [7]. Bacteria such as the group A streptococcus *Streptococcus pyogenes* have evolved surface proteins with the ability to bind to the Fc-region on antibodies with high binding energy, i.e. affinity. By binding up the Fc-region on the antibody, the bacteria can no longer be detected via Fc-receptors on phagocytic cells. Hence, they can survive in the host organism. Some common IgGFc-binding proteins on *Streptococcus pyogenes* are the M and M-like protein, protein M1 and protein H respectively [8]. Protein M1 and protein H are long, quite rigid proteins with a coiled structure. They each exhibit one Fc-binding site [9].

Study [1] has shown that the orientation of IgG on the surface of *Streptococcus pyogenes* differs in samples from saliva and plasma. Electron microscopy images show that IgG is more likely to bind via Fc in saliva, whereas in plasma IgG is more inclined to bind via Fab. (see Fig. 1). The IgG concentration is 10 000 times higher in plasma than in saliva. The results imply that the binding tendencies of antibodies to bacterial surface proteins depend on the concentration of antibodies present.

In the presence of IgGFc-binding regions the binding between bacterial surface proteins and antibodies becomes more complex. As previously mentioned, the Fab-regions vary between clones of antibodies depending on what antigen they are designed to recognize. The Fc-region is roughly the same for antibodies relevant to a bacterial infection [3]. The binding depends on the total concentration of IgG, concentration of the different IgG clones, the concentration of bacterial surface proteins, number of Fab-binding sites, location of epitopes and binding energies to these locations. A theoretical model for describing this competitive binding system has previously been designed. In brief, the Fc-binding affinity is constant and there exists a broad spectrum of Fab-binding affinities to a larger number of binding sites. Thus, with an increase of concentration of antibodies, the probability of high-affinity Fab-binding increases to and extent where the Fc-binding becomes effectively meaningless [10].

The Fc-binding sites on protein M1 and protein H are known [11] [12] but there exists little information on their Fab-epitopes. In the previous model, they have been randomly distributed on the protein. To further our understanding of these binding patterns, it is of interest to localise these epitopes. Are the high affinity Fab-epitopes generally localised close to or far away from the Fc-binding region?

We want to develop a method for localisation of binding regions on M and M-like proteins. Although a very high resolution can be attained with EM imaging, quantification would be difficult to achieve on a larger scale. The aim of this study is to evaluate whether or not stimulated emission depletion (STED) and stochastic optical reconstruction microscopy (STORM) are viable optical techniques for molecular quantification and relative localization studies of bacteria-bound antibodies. The project includes learning these imaging techniques, collecting relevant data and executing the necessary analyses of the images.

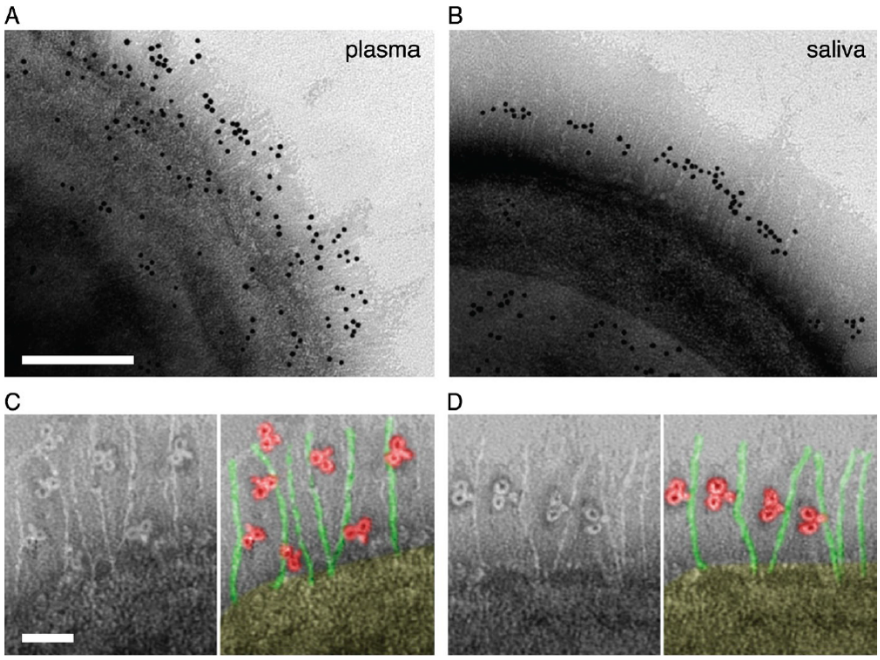

Figure 1: Negative staining electron microscopy (EM) images of IgG bound to *S. pyogenes* in plasma (A and C) and saliva (B and D). The orientation of bound IgG is evident in higher magnification (C and D). In saliva IgG appears to be aligned at Fc-binding regions, located around the middle of both protein M1 and H. In plasma however, IgG binds to many different epitopes via Fab on the bacterial surface proteins. Scale bars: 100 nm (A and B), 25 nm (C and D). Colouring in C and D is added for illustrative purposes. The figure is taken from [1].

There already exist different techniques for localisation of binding sites on proteins. This project specifically seeks a method that is experimentally simple and can produce results in a short amount of time.

The group A streptococcus *S. pyogenes* is estimated to be at the root of at least 700 million skin and throat infections annually [1]. These infections are normally uncomplicated and treatment with antibiotics is generally straightforward [13]. Approximately 3–5% of throat infections may however develop into the more serious condition rheumatic fever [9]. Additionally, *S. pyogenes* can cause rare but serious invasive blood infections with high mortality rates. According to recent estimates there are more than 0.5 million deaths annually due to group A streptococcal infections [14]. As of today, there exists no vaccine against *S. pyogenes*.

Previous findings show that M and M-like proteins play a major role in group A streptococcal infections. Mutants lacking M and M-like proteins seem unable to survive in human blood [9]. In addition to the Fc region on IgG, M proteins can bind other human immunological proteins such as fibronectin, fibrinogen, C4BP and factor H [15]. A greater understanding of the mechanisms by which M-proteins exert their virulence is thus of importance for treatment-oriented research. Knowledge of how our immune system interacts with pathogens may in the future assist in pharmaceutical development.

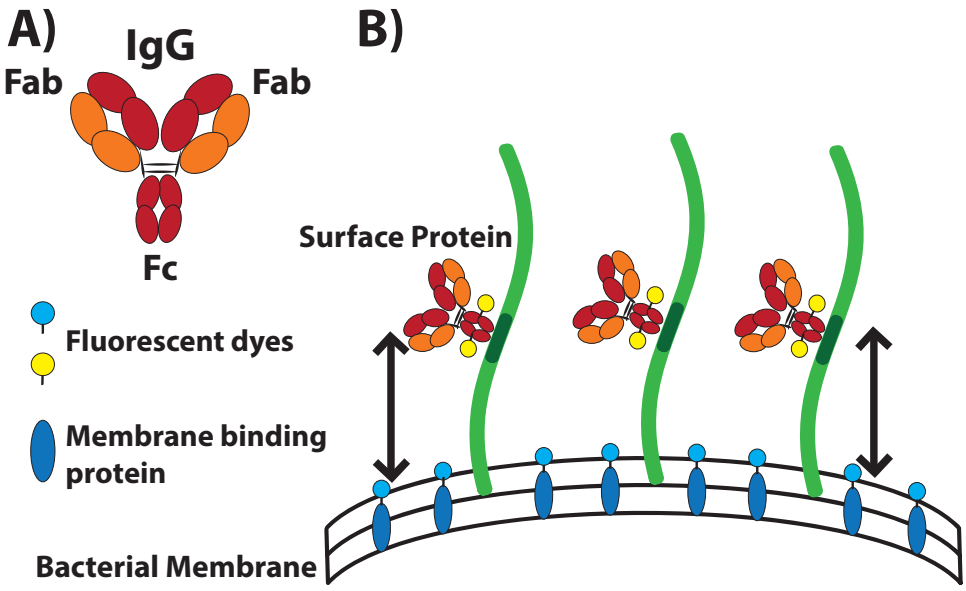

Figure 2: Antibodies bound to bacterial surface proteins. A) shows a schematic figure of an IgG antibody. The Fc region and two Fab regions are marked. B) depicts a segment of a bacterial surface. IgG is bound to the IgGFc-binding region on bacterial surface proteins. A membrane binding protein is bound to the bacterial membrane. This project aims to develop a method to localise binding sites on bacterial surface proteins using super-resolution imaging. This will be done using the IgGFc-binding site on bacterial M-protein as its location is known beforehand. The membrane is adopted as a reference region. The antibody and membrane binding protein are thus labelled with appropriate fluorescent dyes and the aim is to determine the distance between these dyes (shown by the black scale).

2 Background

The following section describes in further detail the concepts, analysis methods and optical systems employed in this project.

The imaging systems used in this project are based on fluorescence microscopy. Fluorophores are fluorescent compounds that can emit light at a specific wavelength upon excitation with a typically shorter wavelength. Fluorescence microscopy is essentially the visualization of fluorescent compounds. For the purpose of biomedical imaging, proteins and other biological structures of interest are labelled with different fluorophores. The sample is irradiated by lasers with wavelengths corresponding to the excitation peak wavelengths of the fluorophores. The emitted light from the samples is detected in different detection channels, enabling differentiation of different structures and separating the emission from the vast background light produced by the excitation laser. This is the basic idea behind fluorescence imaging. A normal setup of this is the widefield microscope, whereas the confocal microscope is a more advanced technique that utilizes optical

sectioning [16]. Details on the techniques relevant for this project are given below in this section.

Relative site localisation will be performed by labelling antibodies and a reference position, such as the bacterial membrane, with a fluorescently labelled protein. The bacteria will be stained with these proteins and can then be imaged.

We attempt to acquire the necessary resolution required for site localisation on M-protein by applying statistical methods and deconvolution on high resolution images. Protein M1 and protein H have a long coiled and rigid structure. In the EM images (see Fig. 1) protein M1 and protein H seem to protrude about 100 nm from the bacterial surface. In order to localise binding sites on these kind of bacterial surface proteins one needs to resolve molecular structures that are less than 100 nm apart. This is not possible with conventional light microscopes and can be challenging even with super resolution optical systems. Therefore, in addition to acquiring super resolution images, deconvolution and statistical methods similar to particle averaging will be employed.

The spatial resolution of a conventional optical imaging system is restricted by the Abbe diffraction limit (see Eq.1). The diffraction limit in the focal plane d_{xy} depends on the wavelength of the excitation laser λ as well as on the numerical aperture NA given by the refractive index n of the medium and the maximal half-angle θ over which the system can accept light. d_z is the diffraction limit along the optical axis [17].

$$d_{xy} = \frac{\lambda}{2n\sin(\theta)} = \frac{\lambda}{2NA} \tag{1}$$

$$d_z = \frac{\lambda}{n\sin^2(\theta)}$$

State of the art lenses typically have a numerical aperture around 1.4–1.6. Since excitation lasers with wavelengths shorter than around 400 nm can cause damage to biological tissue they are not used. Thus, diffraction limited light microscopy can at most achieve a resolution between 250 – 300 nm [16].

Imaging techniques capable of overcoming Abbes diffraction limit are collectively referred to as super resolution techniques. There exist several kinds of super resolution techniques that are based on different principles [18]. The following sections describe the main features of the super resolution techniques employed in this project, namely STED and STORM.

2.1 STED

In Stimulated Emission Depletion (STED) imaging, the excitation laser in a laser scanning confocal system is overlaid by a doughnut-shaped STED laser that depletes the excited states in the coinciding regions of the two lasers. Consequently, the focal spot from which a fluorescence signal can be detected is minimised and the spatial resolution is thereby enhanced.

In a fluorescence microscope, excitation light normally excites a fluorescent molecule, i.e. a fluorophore, from a low vibrational level L_0 of its ground state S_0 to a directly excited level L_1 of its first excited state S_1 (see Fig. 3). It is then relaxed to level L_2 of state S_1 from which it can spontaneously transition to level L_3 of state S_0 and thereafter relax back to level L_0. Emitted light from the transition between level L_2 and L_3 is detected by the optical system [17]. The excitation light, causing the transition L_0–L_1 originates from a laser focused by lenses on to the sample. The emitted light in a confocal microscope is sent through a pinhole prior to detection, ensuring that only light from the focal point is being detected. In the focal plane of the lens, the intensity distribution of the excitation light succumbs to diffraction and can be described by the point spread function (PSF) h_{exc}. The spatial resolution of a fluorescence microscope is determined by the spatial extent of h_{exc} [19].

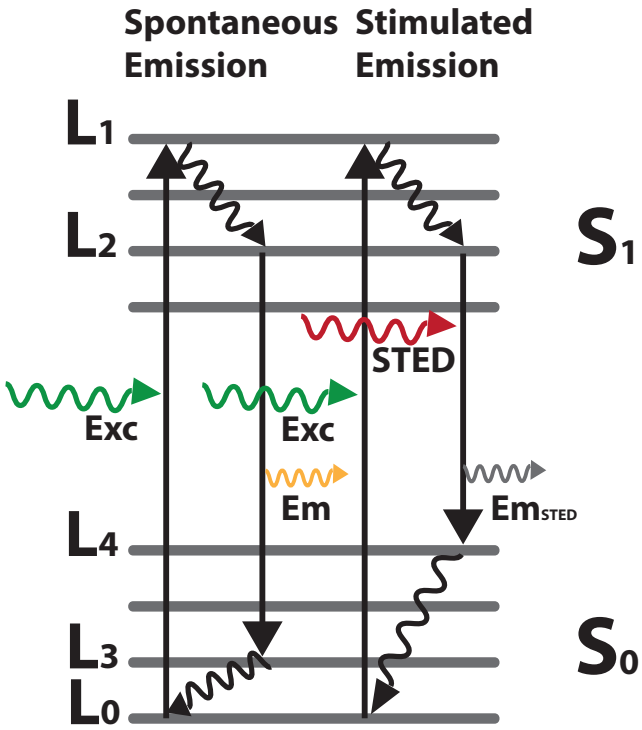

Figure 3: Energy level diagram illustrating spontaneous and stimulated emission. In classical fluorescence microscopy only spontaneous emission occurs (shown to the left). An incoming excitation photon excites the fluorophore to L_1 in S_1 and emits another photon when relaxing back to a low vibrational level L_3 in S_0. In STED imaging, an additional pulsed laser is present that stimulates emission to a different vibrational level L_4. The outer regions of the focal spot in a STED microscope are depleted in this manner, producing a smaller FWHM of the focal spot and thereby increasing the resolution.

Stimulated emission is the process by which an incoming photon causes an electron to drop to a lower energy level, emitting a photon with identical frequency, phase, polarization and direction to that of the incoming photon [17].

In stimulated emission depletion microscopy the spatial extent of h_{exc} is reduced by introducing

an additional laser beam — the STED beam. The STED beam has an intensity distribution h_{STED} that overlaps with the outermost areas of that of the excitation beam h_{exc} [20]. h_{STED} has an intensity profile with a central zero. Thereby, the STED beam can inhibit fluorescence in the outer regions of h_{exc} by inducing a transition from S_1 to S_0 by stimulated emission and depleting the excited state before fluorescence by spontaneous emission can take place. This way, only the innermost region of the distribution h_{exc} gives rise to fluorescence and the full width at half maximum (FWHM) of h_{exc} is effectively reduced [21].

Stimulated emission with a longer STED beam wavelength than the excitation beam wavelength causes electrons in the excited level L_2 to drop to a higher energy level than L_3, denoted L_4 [22]. The photons produced by stimulated emission will most likely have the same vector of propagation as the incoming photon, whereas the photons produced by spontaneous emission are radiated in all directions. This enables the separation of the stimulated emission and the spontaneous emission. The efficiency of the stimulated emission depends directly on the number of incoming photons from the STED beam, i.e. the laser intensity [23]. However a too high laser intensity may destroy the fluorophores. This kind of fluorophore damage is called photobleaching [24].

For most fluorophores, spontaneous emission typically occurs within nanoseconds of the excitation event. This yields a short time window in which stimulated emission can occur. Moreover, the cross section for stimulated emission σ is small. Therefore, a high flux of stimulating photons is required. As an example, a 4 ns excited state lifetime and $\sigma = 25cm^2/J$ requires a light intensity of $10MW/cm^2$ to deplete half the fluorescent states of a fluorophore. A too high intensity causes photobleaching. This is why most STED systems today used a pulsed laser. Pulsed lasers reduce the total energy pumped into the sample [25].

The STED beam is doughnut-shaped [21]. Most STED systems today apply a STED beam in the shape of a torus, generated by a spatial light modulator that can alter the phase, polarization and amplitude of the incoming beam. Theoretically, the STED technique can yield a resolution of molecular size. In reality the resolution is limited by the signal to noise ratio (SNR) and a lateral resolution of 30–80 nm can typically be attained [26], although; a resolution of 2.4 nm has reportedly been measured [27].

For optimal SNR the alignment of the STED beam and excitation laser should be precise, the STED beam intensity at the focal point should be minimal, suppression of fluorescence by the STED beam should be maximised and the photobleaching minimised. The latter two factors depend on the STED beam wavelength as well. A wavelength close to the emission peak of the fluorophore yields a larger cross section for stimulated emission but may give rise to unwanted excitation by the STED beam [25].

The sub-diffraction resolution attained by STED can be derived from the excitation probability h_{exc} and the intensity distribution h_{STED}. They are given by

$$h_{\text{exc}}(r) = cos^2\left(\frac{\pi r n \sin\theta}{\lambda_{exc}}\right) \tag{2}$$

$$h_{\text{STED}}(r) = I\sin^2\left(\frac{\pi r n \sin\theta}{\lambda_{STED}}\right) \tag{3}$$

where r is the distance from the centroid of the focal point, I is the maximum STED intensity, λ_{exc} and λ_{STED} is the wavelength of the excitation beam and the STED beam, respectively.

After a focal volume has been exposed to a STED pulse, the probability of fluorescence in the focal volume decays to

$$\eta(r) = exp[-\sigma t_s h_{\mathrm{STED}}(r)] \tag{4}$$

where t_s is the pulse duration. The intensity distribution of the effective spot is $h(r) = h_{\mathrm{exc}}(r)\eta(r)$. Inserting Eq.2, Eq.3 and Eq.4 in to this and approximating $\lambda_{exc} \approx \lambda_{STED} = \lambda$ yields

$$h(r) \approx \cos^2\left(\frac{\pi r n \sin\theta}{\lambda}\right) exp[-I\sigma t_s \sin^2\left(\frac{\pi r n \sin\theta}{\lambda}\right)] \tag{5}$$

Taylor expansion to second order at $r = 0$ gives

$$h(r) \approx 1 - \left(\frac{\pi r n \sin\theta}{\lambda}\right)^2 (I\sigma t_s + 1) \tag{6}$$

The FWHM is obtained by solving 6 for r at $h(r) = 0.5$;

$$r = \pm\frac{\lambda\sqrt{0.5}}{\pi n \sin\theta\sqrt{I\sigma t_s + 1}} \tag{7}$$

Thus

$$\Delta r = 2\frac{\lambda\sqrt{0.5}}{\pi n \sin\theta\sqrt{I\sigma t_s + 1}} \approx \frac{\lambda}{2n \sin\theta\sqrt{I/I_{sat} + 1}} \tag{8}$$

where $2\sqrt{0.5}/\pi$ was approximated as $1/2$ and the saturation intensity $I_{sat} = 1/\sigma t_s$ was introduced. Eq.8 is the expression for the sub-diffraction resolution of STED.

STED is a deterministic functional technique as it utilizes the non-linear response of fluorophores to enable image acquisition with a sub-diffraction resolution, whereas STORM is a stochastic functional technique that adopts a mathematical model to reconstruct images after acquisition [28].

2.2 STORM

In Stochastic Optical Reconstruction Microscopy (STORM) imaging single fluorophores are localised through sequential activation of photoswitchable probes. Thousands of images are captured of the same field of view and a resulting image is reconstructed by summation and centroid localisation of all detected single fluorophores.

STORM relies on photoswitchable fluorophores [29]. Fluorescent dyes that can reversibly switch between "on" fluorescent state and "off" non-fluorescent state are called photoswitchable. The transition rates for these states are k_{on} and k_{off}. The number of molecules in either state on or off, N_{on} and N_{off} in equilibrium is related to the transition rates as

$$\frac{N_{\mathrm{on}}}{k_{\mathrm{on}}} = \frac{N_{\mathrm{off}}}{k_{\mathrm{off}}} \tag{9}$$

This ratio determines the number of active fluorescent molecules per area [30].

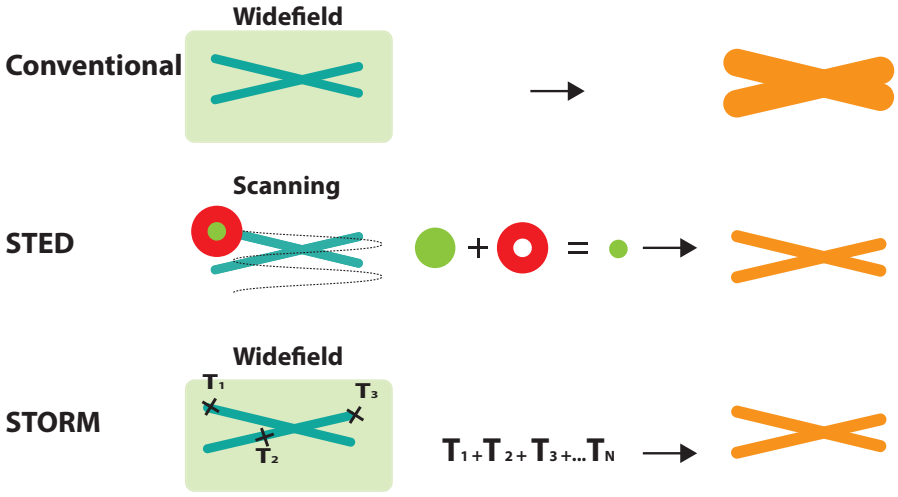

Figure 4: Schematics of the main concepts behind STED and STORM imaging compared with conventional fluorescence microscopy. The sample is illustrated on the left side. STORM is based on a widefield system in which the entire sample is illuminated at any given time whereas STED is a confocal laser scanning technique. In STED, the excited states of the fluorophores are depleted by stimulated emission in the outer regions of the focal spot by the doughnut-shaped STED beam. A large number N of single photoswitching events are captured by the STORM system and thereafter reconstructed with centroid localisation of each event, resulting in one high resolution image.

The principle of STORM is to localise the centroid of fluorophores from several switching cycles. To do this, we must ensure that isolated single fluorophores are being imaged. Using the photoswitchable property of certain fluorophores, we can ensure that we are seeing only a few fluorescent molecules at a time and not a blur consisting of many overlapping fluorophores. In a conventional microscope image of an isolated nano-scale fluorophore the FWHM of the intensity distribution will be a few hundred nanometers. It is nevertheless possible to say that the position of the fluorophore is centered at the peak of the imaged intensity distribution. By fitting a distribution to the imaged fluorophore, its true position can be determined with a precision limited only by the number of photons collected [28]. The standard deviation σ of the precision measurement is given by

$$\sigma \approx \sqrt{\frac{s^2 + a^2/12}{N} + \frac{4\sqrt{\pi s^3 b^2}}{aN^2}} \tag{10}$$

where s is the standard deviation of the measured PSF, a is the edge size of the area imaged on each Charge Coupled Device (CCD) pixel, b is the standard deviation of the image background and N is the number of photons detected from the emitting fluorophore [31]. It has been shown that the position of a fluorescent dye can be determined with a precision of about 1.5 nm [32]. The precision in single-molecule localization does however not convert directly into image resolution. Theoretically, an infinite spatial resolution can be attained using this technique. In reality however the resolution is limited by the size, form and variance in space of the fluorophores. A resolution of about 20–30 nm is thus achievable with STORM. It is essential for the quality of the

images that the ratio of activated fluorophores at a given time is sufficiently low for them to be isolated. In order to obtain a complete image, all fluorophores in the specimen must be localised. A couple of thousand images are captured of the same region of interest while the fluorophores are photoswitched and a complete image can thereafter be reconstructed by summing all the molecules localised by centroid fitting [29].

A STORM system normally uses a widefield microscope in total internal reflection fluorescence (TIRF) mode. In contrast to confocal microscopy, the total sample is illuminated at a time in widefield microscopy. TIRF relies on the total internal reflection of light in the sample-glass medium and restricts the excitation to a thin region of the sample [33]. The system is coupled to an electron multiplying (CCD) that can detect single photon events with a faster readout than a traditional CCD.

Direct STORM (dSTORM) was implemented in this project. Photoswitching can be obtained by conjugating two fluorophores with different excitation wavelengths to one another. dSTORM is a technique wherein single fluorophores are manipulated to be photoswitched. Photoswitching is attained and stabilized by using a high power STORM laser and by adding various substances to the specimen. Using imaging buffers with oxygen-scavenging chemicals such as glucose oxidase and quenching certain energy states with mercaptoethanol can help attain and stabilise photoswitching [30].

There are several differences between STORM and STED, making them suited for different purposes. As some excited states are depleted in the STED system, the efficiency of fluorophore-excitation is higher in STORM than in STED. Moreover, since the excitation and depletion lasers scan through the sample in a STED system, the sample is exposed to high beam intensity. Although the STORM laser intensity is quite high it is distributed over a larger area at all times. These factors lead to an increased rate of photobleaching when imaging with STED. An advantage of STED is that the choice of fluorescent dye is not limited by the whether or not it is photoswitchable [24]. Although the theoretical spatial resolution of STORM is higher than that of STED, STORM imaging depends highly on the sample preparation, fluorophores used and the imaging buffer [34]. The STED imaging resolution depends on the photon count of the STED beam whereas the STORM imaging resolution depends on the number of photons captured.

2.3 Deconvolution

In any optical system, there exist several sources of systematic error. A signal from an object under investigation can be shifted or delayed by various components in the optical system. Convolution is a mathematical operation that can accurately describe how intrinsic aberrations modify the input signal. The inverse operation, deconvolution, can therefore be used as a means to retrieve the original object information in images after acquisition. The Richardson-Lucy algorithm for restorative deconvolution was employed in this project [35].

Convolution c of the two functions f and g, denoted $c = f * g$, is the integral of the product between f and a shifted and reversed function g . Explicitly,

$$c = (f * g)(a) = \int_{-\infty}^{\infty} f(\alpha)g(a - \alpha)d\alpha \tag{11}$$

where α is a spatial domain variable and a the variable offset. With restorative deconvolution the aim is to construct the original image f from the acquired image c by a measured or theoretical point spread function (PSF) g [35]. In reality, the PSF is difficult to know exactly and the acquired image is better described as $C = f * g + \epsilon$ where ϵ is some sort of noise in the system. Richardson-Lucy is an iterative algorithm used for deconvolution of images with the form C. The algorithm presumes ϵ to be Poisson-distributed which is an appropriate assumption for photon noise [36] [37]. Based on Bayes theorem, the Richardson-Lucy algorithm attempts to find the maximum-likelihood solution using a given PSF and the noise distribution [35].

2.4 Particle averaging

Particle averaging is a method in which information from a large number of similar particles is used to interpret the structure of each individual one [38].
Individual particles normally have a lower signal-to-noise ratio (SNR) than the summation of many similar particles. By combining data from several particles of the same kind, structures in the particles become more distinguishable from the noise. After imaging, individual particles are identified, structurally aligned and their data is summed. The mean intensity data from this result is the interpretation of each individual particle. This is a straightforward technique for identical particles. The structure of interest in this project is similar in all *S. pyogenes*, but each cell may vary somewhat in shape and size. However, after certain transformations a method based on the concept of particle averaging can be employed. This is explained in further detail in section 3.3.

Particle averaging is routinely used in EM-imaging [38]. Super resolution microscopy and particle averaging have previously been combined to investigate the structure of nuclear pore scaffolds with a position precision well below 1 nm [39]. Additionally, the surface proteins of herpes simplex virus type-1 were analysed using STORM and particle averaging [40].

3 Methods and Analysis

As previously stated, this project aims to develop a method to localise binding sites on bacterial surface proteins using super-resolution microscopy. We attempt this by using the IgGFc-binding site on bacterial M protein as its location is known beforehand [12]. Experimentally, any IgG antibody clone with very low Fab-affinity to *S. pyogenes* will only bind to the Fc-region. The membrane is adopted as a reference level for this relative localisation study (see Fig. 2) An appropriate IgG clone and membrane binding protein, labelled with different fluorophores, was thus prepared for imaging and captured in both the STORM and STED system. Several membrane binding proteins and fluorophores were tried out during the course of this project. It was essential to find fluorophores that were compatible with both STED and STORM as well as a membrane dye that was specific. Ultimately, the membrane dye mCLING [41] conjugated to the fluorophore Alexa Fluor 594 was used. The antibody clone utilised was Xolair labelled with AlexaFluor647 using GlyCLICK^{TM} (Genovis AB) technology. GlyCLICK^{TM} enables site specific conjugation to the Fc-domain of an antibody and ensures a labelling factor of two fluorophores per antibody (schematically illustrated in Fig. 2). mCLING was conjugated to Alexa Fluor 594 according to a standard labelling kit protocol (see appendix A.1).

It is important to note that with fluorescence microscopy, the signal of the fluorophore is obtained. Therefore it is crucial that the fluorophores are as close as possible to the actual location of interest. Consequently, no secondary antibodies have been used in this project; the proteins of interest are directly conjugated. Moreover, the labelling site specificity achieved with GlyCLICK^{TM} is highly advantageous for precise localisation.

Section 3.3 describes the method for analysing the images to resolve mean distance between the membrane and the bound antibodies. This method was implemented in the dynamic programming language Julia [42].

3.1 Sample Preparation

This section describes in short how samples were prepared for imaging. For additional details, protocols can be found in appendix A.1.

To begin with, bacterial cultures of the *S. pyogenes* strains MC25 and AP1 were grown to their exponential phase. They were then heat-killed by incubation at 80 °C for 5 minutes followed by immediate cooling by placing them on ice. Because we are only interested in the binding characteristics of bacterial surface proteins, it is not necessary to keep these pathogenic *S. pyogenes* strains alive. It has been showed in previous publications that the surface proteins interactions remain intact after heat-killing of bacteria [1]. Each heat-killed strain was allocated into 4 samples; two samples to be labelled by both the membrane protein and antibody as well as two controls containing only either one of the proteins.

Fluorescently labelled membrane protein was then added to the appropriate samples and incubated for the required time. Remaining unbound membrane protein was washed away by centrifuging down the samples, eliminating the supernatant and adding fresh medium. Xolair antibodies were then added to the appropriate samples and incubated for 30 minute5s. Once the samples had been stained, they were fixated using 4% paraformaldehyde and 0.2% glutaraldehyde. The fixation medium was washed away and the samples were ready to be mounted for imaging.

For STED imaging, the samples were mounted on fibronectin-coated coverslips. No. 1.5 glass coverslips were coated overnight with a solution of fibronectin for the purpose of increasing bacterial adherence. The samples were placed on the coverslips for a couple of hours. Remaining liquid was thereafter removed and mountant with photobleach-reducing properties was added. The coverslip was placed on a glass slide and was left to dry overnight.

For STORM imaging, the samples were set on dishes with coverslip bottoms. As with the STED samples, the coverslips were coated with a solution of fibronectin overnight. The samples were thereafter placed on the dishes. An imaging buffer was added to the dish during acquisition to enhance photoswitching (see appendix A.1). This contains various substances and acts as an oxygen scavenging medium. Several different protocols were tested during the course of this project with the aim to optimize the photoswitching. The mixture that was ultimately used consisted of a basic protocol with the addition of cyclooctatetraene (COT) (see appendix A.1) [43].

3.2 Image acquisition

The following section presents some main aspects of the image acquisition such as system calibration and control imaging.

Prior to taking images with the STED system, gold beads were viewed through the microscope. These reflect the incoming light and therefore accurately represent the position of the lasers. The STED beam and excitation laser alignment was adjusted if required. Moreover, the shape of the STED laser was examined and modified if necessary. Technical properties of the system, such as the laser powers and the pinhole, typically needed to be adjusted for each unique sample.

Occasionally when imaging with STORM, the samples need to be bleached before images can be captured to lower the ratio of "switched on" molecules (see Eq.9). This was done by a few minutes exposure to the high power STORM laser. About 10 000 shots were captured of each field of view for the STORM images.

The prepared samples were imaged with both systems. The membrane fluorophore and the antibody fluorophore have emission peak wavelengths of 594 nm and 647 nm, respectively. They are excited with appropriate excitation lasers and viewed in different spectral channels. An additional activator-laser with lower wavelength was present for each fluorophore in the dSTORM system. Control sample images were captured to investigate whether or not there was any emission overlap in the detection channels.

The FWHM of the PSF was estimated for both systems by capturing sub-resolution sized beads and measuring their FWHM.

3.3 Image analysis

The following section describes how the images were analysed to resolve a mean distance between the membrane and the bound antibodies. The supplementary code can be found in appendix B.

STORM images were reconstructed using the ThunderSTORM software [44]. Thereafter, the STED and STORM images were analysed in the exact same manner, allowing a precise comparison. The effect of deconvolution was evaluated by performing varying number of iterations with the Richardson-Lucy algorithm.

Single bacteria were detected in the image. Circular patterns were identified using the Circle Hough Transform [45] in one channel by first performing a Canny Edge Detection [46]. Masks slightly larger than the identified circles were isolated for each bacteria. The data in these masks were polar transformed, i.e. represented as the radii and discrete angle of the mask.

To extract the mean distance between the membrane and the binding site, an alignment of the membrane position was performed by fitting Gaussians to each intensity profile and identifying the peak positions. The membrane position alignment was thereafter used to transform and shift the corresponding data in the antibody channel. As some bacteria were attached to one another, their surface data was superimposed and hard to separate. Therefore the data of the overlapping angles were identified and eliminated.

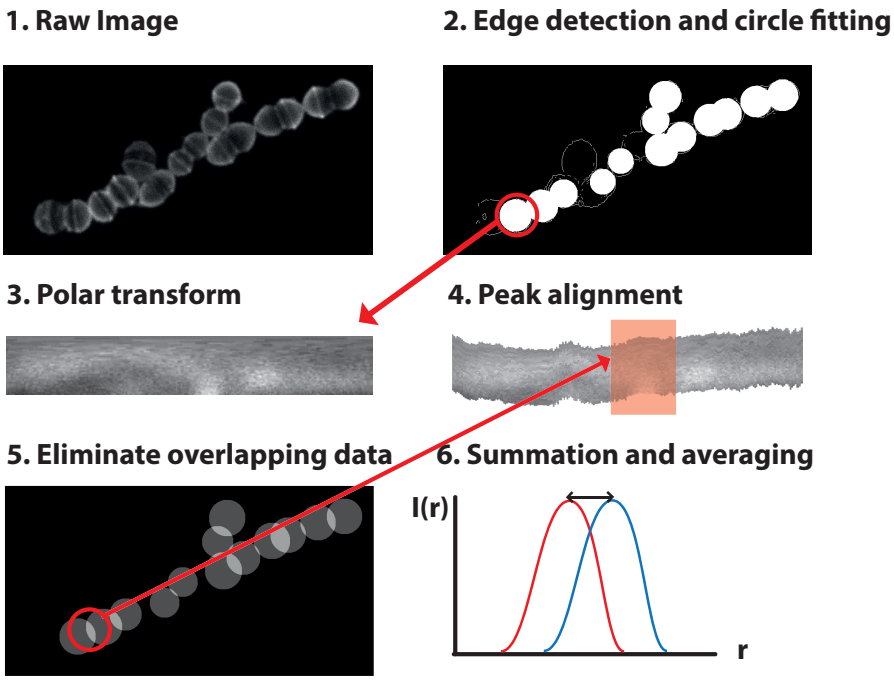

Figure 5: Extracting the mean distance between antibodies and membrane. 1. One of the channels is chosen as the reference data. 2. Single bacteria are identified by fitting circles to an edge-detection-processed image. 3. Each circle is isolated as a slightly larger mask and the data is polar transformed. 4. An alignment of the membrane position is performed by fitting Gaussian to each intensity profile and identifying peaks. 5.+ 6. Overlapping data is removed prior to summation and averaging of the intensity profiles. The corresponding data in the other channel is processed in the same manner.

As with particle averaging, the intensity profiles from each bacterial particle were summed separately in both channels, normalised and a summation of all identified particles was calculated. The mean intensity and precision of the distance between the distributions of the two channels was calculated for different data sets. Each bacteria was weighted according to its number of data points. Because some samples had a higher background intensity from inside the bacteria their intensity distribution was asymmetrical. An intensity cutoff was introduced for these data sets.

4 Results

The following section presents the results from imaging and analysis in this project. An example of STED images together with their corresponding confocal images is shown in Fig. 6. Plots depicting mean intensity profiles of confocal and STED images from the same dataset are shown in Fig. 7. Additionally, mean intensity profiles of this dataset deconvolved with the Richardson-Lucy algorithm are presented in Fig. 7. A reconstructed STORM image is shown in Fig. 9 and Fig. 10 shows a STED and STORM image of the same sample beside one another. Averaged

and normalised intensity profiles for STED and STORM are shown in Fig. 11.

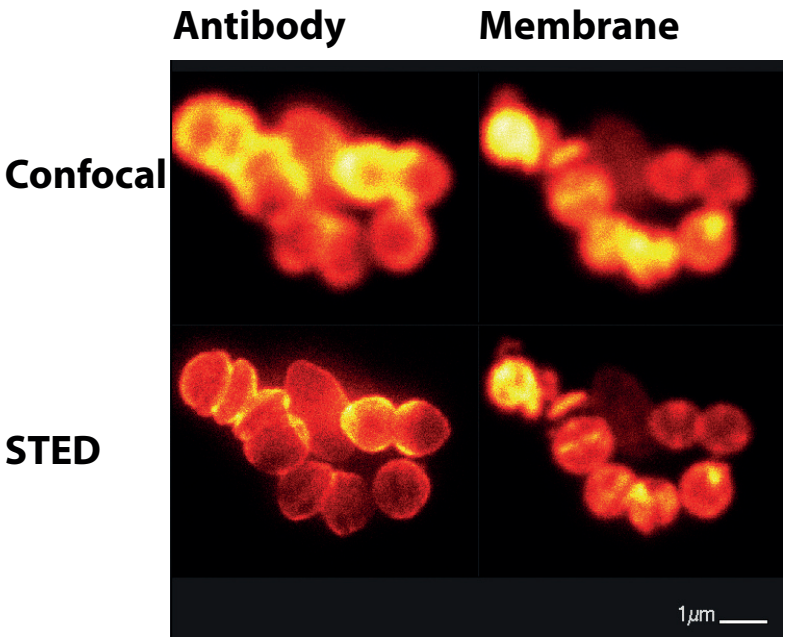

Figure 6: A representative example of images captured with the STED system. The top two images are acquired using the regular laser scanning confocal system while the bottom two are STED images. The images to the left represent signal from the detection channel for AlexaFluor647-labelled Xolair antibodies whereas the right images represent signal from the detection channel for AlexaFluor594-labelled membrane binding protein mCLING. All four images depict the same set of bacteria. Finer structures are resolvable in the STED images and the confocal images are blurry in comparison.

An example of STED images is shown in Fig. 6. The MC25 strain was prepared with AlexaFluor647-labelled Xolair antibodies and AlexaFluor594-labelled mCLING. The two different detection channels are presented separately. The STED images are shown with their corresponding confocal images and clearly the STED images exhibit more detail than the confocal images. For these fluorophores, the crosstalk between the detection channels was negligibly low in comparison with the signal.

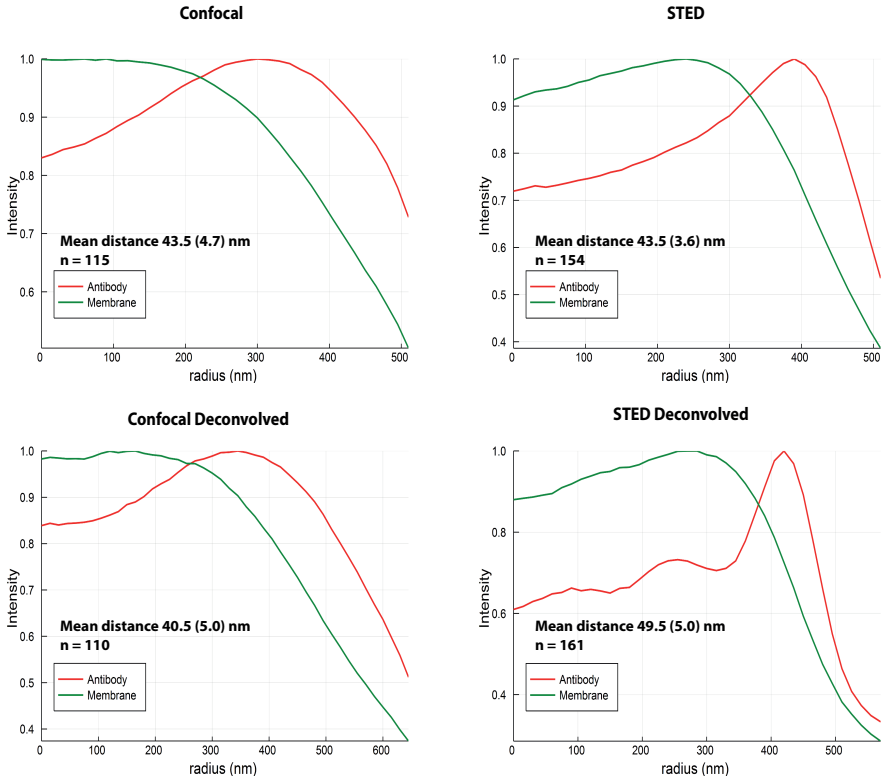

Figure 7: Averaged and normalised intensity profiles of STED and confocal images of the same datasets. Each plot depicts the averaged intensity profile along the radii of the bacteria. The x-axis is the radius given in nanometers (nm) and the y-axis is the normalised intensity. The green and the red curve represent the membrane (AlexaFluor594-labelled mCLING) and antibody (AlexaFluor647-labelled Xolair) intensity distributions respectively. The top left plot shows the intensity distributions acquired from the confocal images while the top right depicts the same for the corresponding STED images. Images have been deconvolved with 100 iterations of the Richardson-Lucy algorithm prior to averaging in the two bottom plots. The number of detected bacteria n and the average distance between the curves together with their confidence interval in brackets is given in each plot.

Fig. 7 presents mean intensity profiles along the radii of bacteria for confocal and STED images before and after deconvolution. All four plots were calculated from the same dataset but due to differences in the input images, a varying number of bacteria n were detected in the plots.

The FWHM of the PSF was measured for the STED system to about 40 nm. The deconvolution for STED was thus performed using a Gaussian PSF with a FWHM of 40nm. The FWHM of the PSF for the confocal images was estimated to be 200 nm. The Richardson-Lucy algorithm converges within 100 iterations for these images.

A t-test was performed for all calculated mean distances to ensure that there in fact was a significant difference between the mean value of the antibody and the membrane distribution. For p-value = 0.05 the null hypothesis - that the mean values of the two distributions are equal- is rejected if $t_0 > t = 2.26$. This was the case for all intensity profiles shown in Fig. 7. The 95% confidence interval CI of the mean distances $\overline{d}$ was thereupon calculated as $CI = tS_d/\sqrt{n}$ where S_d is the weighted standard deviation of $\overline{d}$. $\overline{d}_{STED}$ was calculated to be 43.5 ± 3.6 and $\overline{d}_{Confocal}$ was calculated to be 43.5 ± 4.7. For the deconvolved images $\overline{d}_{STED}$ and $\overline{d}_{Confocal}$ was 49.5 ± 5.0 and 40.5 ± 5.0 respectively.

The distributions for the STED images (see Fig. 7) appear more narrow than the distributions for the confocal images and both seem to become slightly more narrow when deconvolved. However, the mean distance and confidence interval are not significantly affected by deconvolution. Perhaps this can be explained by the varying n in the different plots.

It is evident from Fig. 7 that the distributions are asymmetrical. Moreover, the example images show that the background intensity inside the bacteria is high, particularly in the membrane channel. This may be because the membrane binding protein mCLING is binding to structures inside the bacteria as well. For comparison, Fig. 8 shows the intensity profile of AlexaFluor647-labelled antibodies with AlexaFluor594-labelled wheat germ agglutinin (WGA) instead of mCLING; these two curves have a similar shape, as opposed to the intensity profiles in Fig. 7. WGA is a protein that binds to structures on the surface of the bacteria. The mean distance between the WGA and the antibody was calculated to be 7.8 ± 5.3 nm suggesting that the proteins bind too close to one another for WGA to be an appropriate protein for this particular relative localisation study.

Reconstructed STORM images are shown in Fig. 9. As with the STED images these samples consist of the MC25 strain prepared with AlexaFluor647-labelled Xolair antibodies and AlexaFluor594-labelled mCLING. The antibody and membrane channels are shown both separately and together. All STORM images were reconstructed from 10 000 consecutive captures using the ThunderSTORM software. The form of the bacteria is more or less perceivable in the antibody channel. This is however difficult in the membrane channel. A similar pattern is evident throughout the two-channel STORM images.

Images from a sample that was split and mounted for both STED and STORM imaging can be seen in Fig. 10. The antibody and membrane channels have been merged in both the STED and STORM image. Signal in the STORM image is localised to focal areas and the two colour channels are spatially distinct from one another. Moreover, the STORM image lacks data at certain points. The STED image has a larger spatial overlap between the two colour channels. The signal in the STED image is overall more complete and smooth. Structures inside the bacteria are resolvable in the STED image but barely in the STORM image.

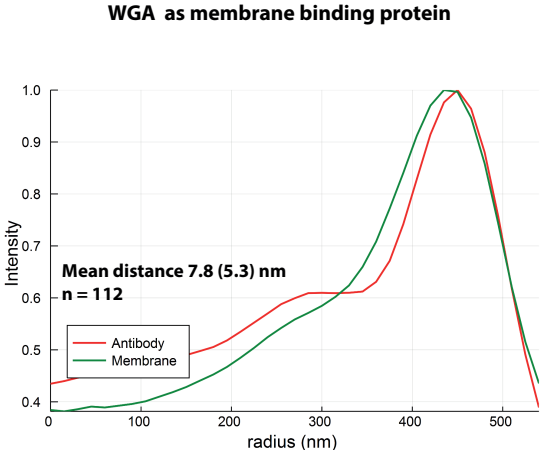

Figure 8: Averaged and normalised intensity profile of STED images of bacterial samples labelled with AlexaFluor594-labelled WGA and AlexaFluor647-labelled Xolair antibodies. The x-axis is the radius given in nanometers (nm) and the y-axis is the normalised intensity. The green and the red curve represent the membrane and antibody intensity distributions respectively. The images have been deconvolved with 100 iterations of the Richardson-Lucy algorithm prior to averaging. The number of detected bacteria n and average distance between the curves together with their confidence interval in brackets is given in the plot.

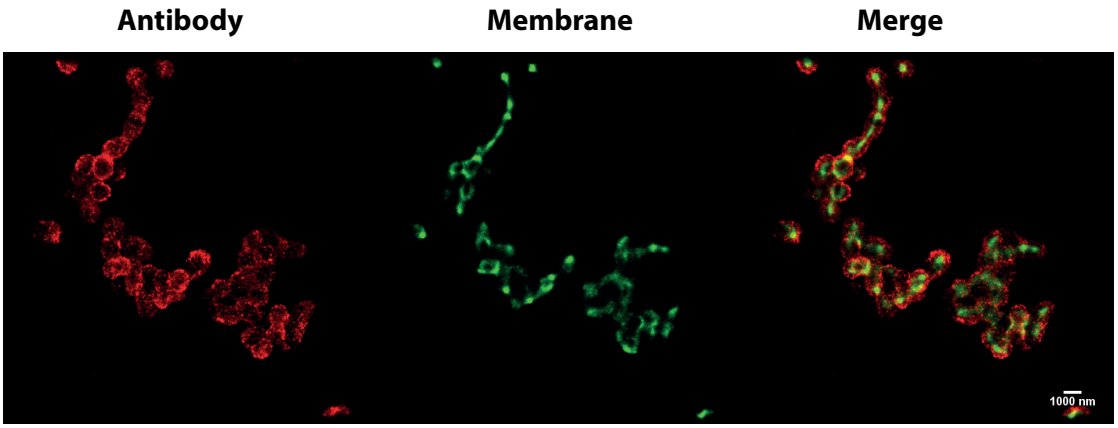

Figure 9: An example of reconstructed STORM images. The red channel to the left depicts the AlexaFluor647-labelled Xolair antibodies, the green channel in the middle depicts AlexaFluor594-labelled mCLING and the right side image is a merge of the two. The image is reconstructed from 10 000 consecutive captures. The bacterial shapes can clearly be identified in the antibody channel but are hard to identify in the membrane channel.

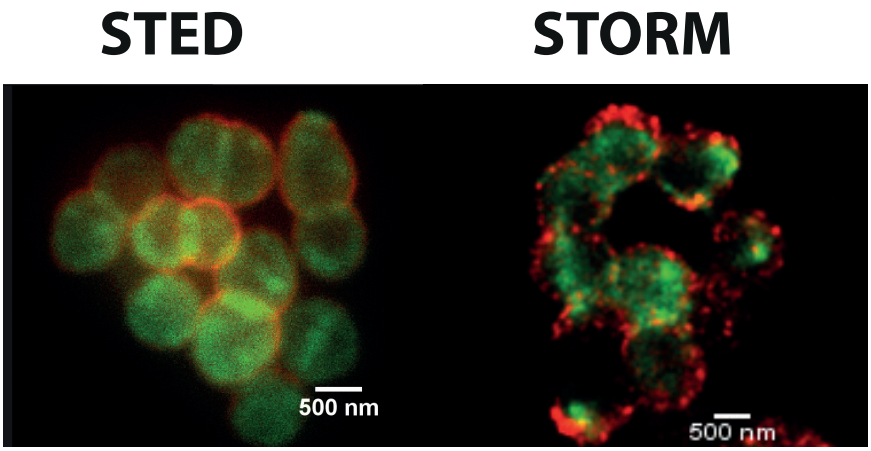

Figure 10: A STED and a STORM image of the same sample are shown beside one another. The green in both images represents the membrane-channel signal while the red represents the antibody-channel signal. The STORM image is reconstructed from 10 000 captures. While the signal from the antibody and the membrane signal in the STORM image are more spatially distinct from one another, the STED image is more complete. The STORM image lacks information in certain areas. There is larger spatial overlap between the antibody and membrane signal in the STED image than in the STORM image.

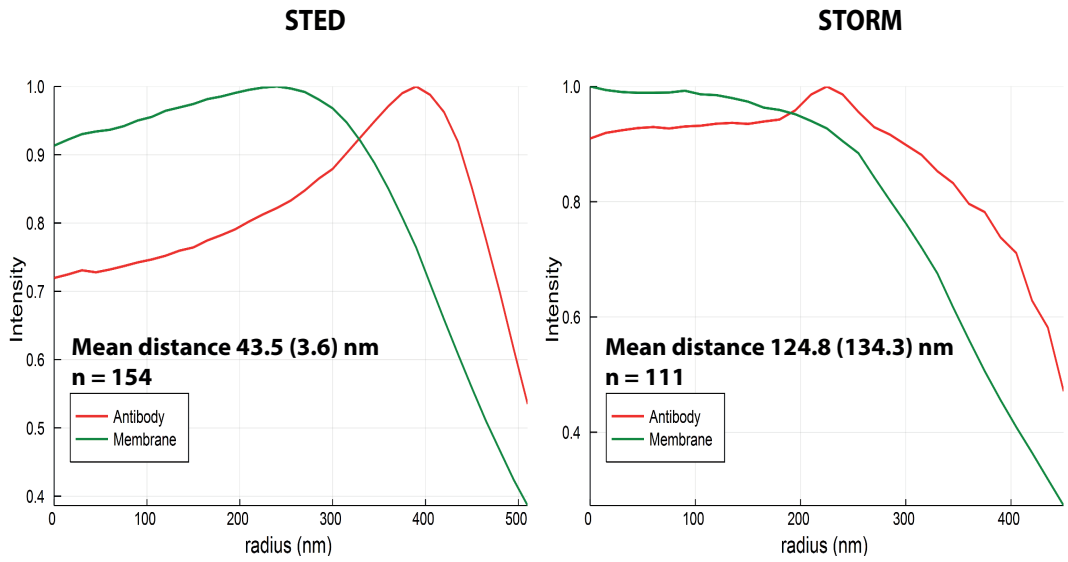

Figure 11: Averaged and normalised intensity profiles of STED and STORM images. Each plot depicts the averaged intensity profile along the radii of the bacteria. The x-axis is the radius given in nanometers (nm) and the y-axis is the normalised intensity. The green and the red curve represent the membrane (AlexaFluor594-labelled mCLING) and antibody (AlexaFluor647-labelled Xolair) intensity distributions - respectively. The number of detected bacteria n and the average distance between the curves together with their confidence interval in brackets is given in each plot.The intensity profiles for STED have previously been shown in Fig. 7 and are depicted here again for comparison with the STORM data.

Averaged and normalised intensity profiles for STED and STORM are shown in Fig. 11. The intensity profiles for STED have previously been shown in Fig. 7. $\overline{d}$ for STORM is calculated to be 124.8 ± 134.3 nm whereas it is 43.5 ± 3.6 nm for STED. As previously discussed, the STORM images lacked some data and certain structures were not resolvable with the STORM. The STORM data did not pass the t-test.

5 Discussion

The results are discussed in this section. The super-resolution imaging techniques STED and STORM are compared to one another in terms of image quality, practicality and, more specifically, for the use of site localisation on bacterial surface proteins.

The aim of this project was to evaluate whether STED and STORM are viable techniques for relative localisation studies on bacterial surface proteins. This was attempted by using antibodies that only bind to the IgGFc-binding site on bacterial M protein and the membrane binding protein mCLING. These proteins were labelled with fluorophores that seemed compatible with both STED and STORM. Several kinds of STED and STORM images were acquired during the course of this project. The mean distance between averaged intensity profiles was calculated using a method based on particle averaging. According to the results, the mean distance between the membrane and the bound antibodies is calculated to be 43.5 ± 3.6 nm in the STED images. Considering the distance seen in Fig. 1, this may be a reasonable result. Roughly speaking, the confidence interval appears to amount to the size of the binding site. The mean distance in the STORM images was calculated to be 124.8 ± 134.3 nm. There may be several reasons for the large difference between the STED and STORM results. To begin with, the STORM system is much more sensitive to artefacts in the image. Furthermore, a too high photoswitching ratio (Eq.9) can decrease the quality of the reconstructed image. A qualitative comparison is illustrated in Fig. 10, showing a STED and a STORM image of the same sample beside one another. Generally, the STED image exhibits more detail. Interestingly, the mean distance determined with the confocal images was 43.5 ± 4.7 nm which agrees with the STED results and has a narrow confidence interval. Even though the standard deviation of the intensity profile distributions was high for the confocal system, the averaging method resulted in a narrow confidence interval. The deconvolved images did not significantly affect the mean distance or confidence interval of the intensity profiles. In fact the CI was increased to 5.0 nm for both the STED and confocal images. Generally the more information a raw image contains, even though it is noise, the more accurate the deconvolution [47]. Due to the pinhole in a confocal microscope and the photoswitching module in STORM, the light intensity is relatively limited. Deconvolution would probably have a more significant effect on conventional widefield images.

In addition to the results in section 4, it is important to evaluate practical aspects of these imaging techniques. Samples could be labelled and fixed in the same manner for both STED and STORM. This was an advantage as it enabled a direct comparison of the results.

STORM imaging requires a precise preparation of the imaging buffer. Photoswitching is very sensitive to the content of the imaging buffer. On several occasions it was not possible to acquire any STORM images and this was most likely due to a slight offset in pH of the imaging buffer. Moreover, several substances regularly included in protocols for STORM imaging buffers are

highly carcinogenic and should not be inhaled. Nevertheless, the imaging buffers must be placed on the sample dish at the time of acquisition and will be in contact with air outside of a safety hood. Additionally, the imaging buffer functions only for a couple of hours before it needs to be replaced.

STED imaging requires calibration to be performed regularly, preferably at the start of each imaging session. The STED system has many properties, such as pinhole size and the power of each laser, that should be adjusted to each sample for optimal imaging. The STORM microscope did not require much preparatory work before imaging.

Each STORM image required about 10 000 captures to produce a reasonable reconstructed image. This could take up to 15 minutes depending on image size. A long acquisition time is disadvantageous if large datasets are a priority. If a only a few number of images are needed, STORM may be the preferred imaging technique as the STED requires more preparatory work.

Despite using a mountant with anti-photobleaching properties for the STED samples they were quite easily bleached. Typically only one image scan could be performed on a particular field of view before that area was completely bleached. Photobleaching was not as pronounced with the STORM system.

In this study, a statistical method based on particle averaging was implemented. When running the analysis, the sensitivity for the Canny Edge Detection and Circle Hough Transform could be increased but this normally compromised the specificity. The method may need to be improved to detect more bacteria without introducing artefacts. This was an issue faced during the analysis and not all imaged bacteria were detected in the analysis. It could be useful to try processing the images in other ways, such as increasing the contrast, prior to circle detection. Gaussians were fitted for peak identification and this seemed to give a reasonable alignment. However, the distance between the maxima in the intensity profiles (see Fig. 7) appears to be larger than the calculated mean distance. The Gaussian fittings may be appropriate for alignment of the bacterial surface, but might not be the most suitable method for calculating the mean distance. The analysis could possibly be improved by the use of a different peak identification method.

6 Conclusion and Outlook

In conclusion, there are various advantages and disadvantages to consider when evaluating the efficiency of STED and STORM. According to our results, STED together with an averaging method, may be an appropriate technique for relative site localisation studies on bacterial surface proteins. Our results also suggest that confocal microscopy together with an averaging method may be a reasonable alternative for relative site localisation.

As discussed in section 5, the analysis may be improved by optimisation of the bacterial detection and implementing a different peak identification method.

It is known that STORM imaging has the potential of reaching high resolutions. Perhaps this requires a more thorough optimisation of sample preparation, image acquisition and analyses. Once this has been achieved, STORM imaging may be the more accessible method. It could be

useful to try other fluorophores or imaging buffers for the STORM.

A future aim is to be able to use an accessible site localisation method to determine binding sites of antibodies with high binding energy to M protein via Fab. This is the dominating kind of binding in plasma (see Fig. 1). This may help in better understanding how M and M-like proteins exert their virulence in the human body and, in the future, assist in pharmaceutical development for *S. pyogenes*. Antibodies with high specificity to M protein are in the progress of being isolated. Even the binding site of other immunological proteins that bind to M protein, such as fibronectin and fibrinogen, may be of interest to localise. The method for relative site localisation could be extendible to other particles or cells. An advantage with this method is that this may be used for irregularly shaped particles as well.

7 Acknowledgements

I would like to thank my supervisors Jason Beech, Pontus Nordenfelt and Jonas Tegenfeldt as well as their respective labgroups for all the support and guidance in this project. A very special thanks to Elke Hebisch for sharing her beaming personality, many insights and all her expertise with the STED. I would also like to thank Sebastian Wasserström and Björn Morén from Lund Bio-Imaging Center (LBIC) for their guidance with the STORM system. A big thanks to my husband Johannes Ahnlide for insisting I use Julia and teaching me how to. Finally, I thank my family for always being there for me.

References

[1]P. Nordenfelt, S. Waldemarson, A. Linder, M. Mörgelin, C. Karlsson, J. Malmström, and L. Björck, "Antibody orientation at bacterial surfaces is related to invasive infection.", The Journal of experimental medicine **209**, 2367–81 (2012).

[2]K. K. M. Murphy, P. Travers, M. Walport, and C. Janeway, *Janeway's immunobiology.* (Garland Science, 2008).

[3]A. K. Abbas, A. H. Lichtman, S. Pillai, D. L. M. illustrator) Baker, and A. Baker, *Basic immunology : functions and disorders of the immune system* ().

[4]L Björck and G Kronvall, "Purification and some properties of streptococcal protein G, a novel IgG-binding reagent.", Journal of immunology (Baltimore, Md. : 1950) **133**, 969–74 (1984).

[5]A Forsgren and J Sjöquist, ""PROTEIN A"FROM S. AUREUS. I. PSEUDO-IMMUNE REACTION WITH HUMAN GAMMA-GLOBULIN.", Journal of immunology (Baltimore, Md. : 1950) **97**, 822–7 (1966).

[6]G Lindahl and G Kronvall, "Nonimmune binding of Ig to Clostridium perfringens. Preferential binding of IgM and aggregated IgG.", Journal of immunology (Baltimore, Md. : 1950) **140**, 1223–7 (1988).

[7]C. H. Sandt and C. W. Hill, "Nonimmune binding of human immunoglobulin A (IgA) and IgG Fc by distinct sequence segments of the EibF cell surface protein of Escherichia coli.", Infection and immunity **69**, 7293–303 (2001).

[8]B. M. Kihlberg, M Collin, A Olsén, and L Björck, "Protein H, an antiphagocytic surface protein in Streptococcus pyogenes.", Infection and immunity **67**, 1708–14 (1999).

[9]V. A. Fischetti, *M Protein and Other Surface Proteins on Streptococci* (2016).

[10]V. Kumra, "Modelling antibody orientation at bacterial surfaces", Lund University Student Papers (2017).

[11]I.-M. Frick, P. Åkesson, J. Cooney, U. Sjöbring, K.-H. Schmidt, H. Gomi, S. Hattori, C. Tagawa, F. Kishimoto, and L. Björck, "Protein H — a surface protein of Streptococcus pyogenes with separate binding sites for lgG and albumin", Molecular Microbiology **12**, 143–151 (1994).

[12]P Akesson, K. H. Schmidt, J Cooney, and L Björck, "M1 protein and protein H: IgGFc- and albumin-binding streptococcal surface proteins encoded by adjacent genes.", The Biochemical journal, 877–86 (1994).

[13]A. Efstratiou and T. Lamagni, *Epidemiology of Streptococcus pyogenes* (University of Oklahoma Health Sciences Center, 2016).

[14]J. R. Carapetis, A. C. Steer, E. K. Mulholland, and M. Weber, "The global burden of group A streptococcal diseases.", The Lancet. Infectious diseases **5**, 685–94 (2005).

[15]M. Reglinski and S. Sriskandan, "Streptococcus pyogenes", in *Molecular medical microbiology* (Elsevier, 2015), pp. 675–716.

[16]S. Svanberg, *Multi-Spectral Imaging from astronomy to microscopy - from radiowaves to gammarays*, 2nd ed. (Lund University, Lund, 2015).

[17]B. E. A. Saleh and M. C. Teich, *Fundamentals of photonics* (Wiley-Interscience, 2007).

[18]T. Müller, C. Schumann, and A. Kraegeloh, "STED Microscopy and its Applications: New Insights into Cellular Processes on the Nanoscale", ChemPhysChem **13**, 1986–2000 (2012).

[19]S. W. Hell and J. Wichmann, "Breaking the diffraction resolution limit by stimulated emission: stimulated-emission-depletion fluorescence microscopy", Optics Letters **19**, 780 (1994).

[20]S. W. Hell, K. I. Willig, M. Dyba, S. Jakobs, L. Kastrup, and V. Westphal, "Nanoscale Resolution with Focused Light: Stimulated Emission Depletion and Other Reversible Saturable Optical Fluorescence Transitions Microscopy Concepts", in *Handbook of biological confocal microscopy* (Springer US, Boston, MA, 2006), pp. 571–579.

[21]S. W. Hell, "Far-field optical nanoscopy.", Science (New York, N.Y.) **316**, 1153–8 (2007).

[22]T. Müller, C. Schumann, and A. Kraegeloh, "STED Microscopy and its Applications: New Insights into Cellular Processes on the Nanoscale**", (1986) `10.1002/cphc.201100986`.

[23]V. Westphal and S. W. Hell, "Nanoscale Resolution in the Focal Plane of an Optical Microscope", Physical Review Letters **94**, 143903 (2005).

[24]J. Tam and D. Merino, "Stochastic optical reconstruction microscopy (STORM) in comparison with stimulated emission depletion (STED) and other imaging methods", Journal of Neurochemistry **135**, 643–658 (2015).

[25]G. Vicidomini, P. Bianchini, and A. Diaspro, "STED super-resolved microscopy", Nature Methods **15**, 173–182 (2018).

[26]S. W. Hell, S. J. Sahl, and M. Bates, "Methods and Applications in Fluorescence From single-molecule spectroscopy to super- resolution imaging of the neuron: a review",

[27]D. Wildanger, B. R. Patton, H. Schill, L. Marseglia, J. P. Hadden, S. Knauer, A. Schönle, J. G. Rarity, J. L. O'Brien, S. W. Hell, and J. M. Smith, "Solid Immersion Facilitates Fluorescence Microscopy with Nanometer Resolution and Sub-Ångström Emitter Localization", Advanced Materials **24**, OP309–OP313 (2012).

[28]M. Bates, S. A. Jones, and X. Zhuang, "Stochastic Optical Reconstruction Microscopy (STORM): A Method for Superresolution Fluorescence Imaging", Cold Spring Harbor Protocols **2013**, pdb.top075143 (2013).

[29]M. J. Rust, M. Bates, and X. Zhuang, "Sub-diffraction-limit imaging by stochastic optical reconstruction microscopy (STORM).", Nature methods **3**, 793–5 (2006).

[30]S. Van De Linde and M. Sauer, "How to switch a fluorophore: from undesired blinking to controlled photoswitching", Chem. Soc. Rev. Chem. Soc. Rev **43**, 1076–1087 (1076).

[31]R. E. Thompson, D. R. Larson, and W. W. Webb, "Precise Nanometer Localization Analysis for Individual Fluorescent Probes", Biophysical Journal **82**, 2775–2783 (2002).

[32]A. Yildiz, J. N. Forkey, S. A. McKinney, T. Ha, Y. E. Goldman, and P. R. Selvin, "Myosin V Walks Hand-Over-Hand: Single Fluorophore Imaging with 1.5-nm Localization", Science **300**, 2061–2065 (2003).

[33]K. N. Fish, "Total internal reflection fluorescence (TIRF) microscopy.", Current protocols in cytometry **Chapter 12**, Unit12.18 (2009).

[34]J. Xu, H. Ma, and Y. Liu, "Stochastic Optical Reconstruction Microscopy (STORM)", in *Current protocols in cytometry*, Vol. 81 (John Wiley & Sons, Inc., Hoboken, NJ, USA, 2017), pp. 12.46.1–12.46.27.

[35]C. Solomon and T. Breckon, *Fundamentals of digital image processing : a practical approach with examples in Matlab* (Wiley-Blackwell, 2011), p. 328.

[36]L. B. Lucy, "An iterative technique for the rectification of observed distributions", **79** (1974).

[37]W. H. Richardson, "Bayesian-Based Iterative Method of Image Restoration*", (1972).

[38] J. J. Frank, *Three-dimensional electron microscopy of macromolecular assemblies : visualization of biological molecules in their native state* (Oxford University Press, 2006), p. 410.

[39] A. Szymborska, A. de Marco, N. Daigle, V. C. Cordes, J. A. G. Briggs, and J. Ellenberg, "Nuclear pore scaffold structure analyzed by super-resolution microscopy and particle averaging.", Science (New York, N.Y.) **341**, 655–8 (2013).

[40] R. F. Laine, A. Albecka, S. van de Linde, E. J. Rees, C. M. Crump, and C. F. Kaminski, "Structural analysis of herpes simplex virus by optical super-resolution imaging", Nature Communications **6**, 5980 (2015).

[41] N. H. Revelo, D. Kamin, S. Truckenbrodt, A. B. Wong, K. Reuter-Jessen, E. Reisinger, T. Moser, and S. O. Rizzoli, "A new probe for super-resolution imaging of membranes elucidates trafficking pathways.", The Journal of cell biology **205**, 591–606 (2014).

[42] J. Bezanson, S. Karpinski, V. B. Shah, and A. Edelman, "Julia: A Fast Dynamic Language for Technical Computing", (2012).

[43] N. Olivier, D. Keller, P. Gönczy, and S. Manley, "Resolution doubling in 3D-STORM imaging through improved buffers.", PloS one **8**, e69004 (2013).

[44] M. Ovesný, P. Křížek, J. Borkovec, Z. Svindrych, and G. M. Hagen, "ThunderSTORM: a comprehensive ImageJ plug-in for PALM and STORM data analysis and super-resolution imaging.", Bioinformatics (Oxford, England) **30**, 2389–90 (2014).

[45] R. C. Gonzalez and R. E. R. E. Woods, *Digital image processing* (Prentice Hall, 2008), p. 954.

[46] J. Canny and J, "A Computational Approach to Edge Detection", IEEE Transactions on Pattern Analysis and Machine Intelligence **PAMI-8**, 679–698 (1986).

[47] W Wallace, L. H. Schaefer, and J. R. Swedlow, "A workingperson's guide to deconvolution in light microscopy.", BioTechniques **31**, 1076–8, 1080, 1082 passim (2001).

A Protocols

A.1 Samples for imaging

This section describes the process of preparing the samples for imaging. The necessary solutions, quantities and procedural steps are given below.

Solutions

- PBS
- monoclonal IgG (Xolair) labeled with AlexaFluor647
- Prolong Gold Antifade Mountant
- Alexa fluor 594 conjugated mCLING
- 4 % formaldehyde
- 0.02% gluataraldehyde
- Heat killed bacteria - *S. pyogenes* strain AP1 and MC25

Prepare Bacteria

- Set overnight culture: AP1 and MC25 is placed in 10 ml Todd hewitt broth and incubated at 37 °C.
- Let grow to exponential phase (about 4 h, OD $0.3 - 0.4$) by adding 200 μl of overnight culture in new tube with 5 ml Todd hewitt broth.
- Centrifuge and wash with PBS 3 times (2000g, 5 minutes, swing out rotor, soft deceleration).
- After first centrifugation resuspend them in 1ml PBS and use eppendorf instead
- heat-kill: 80°C for 5 mins in heat block (agitation at 800 rpm). Set on ice.

Sample preparation

1. Add 250 μl of heatkilled bacteria to 250 μl PBS
2. Sonicate bacterial samples using 75% 0.5 cycle, (4 min for AP1). pause for 10 seconds after eac minute to prevent overheating.
3. Check bacteria in microscope, repeat if necessary.
4. Create 3 bacterial samples of 100 μl (AP1 + PBS) and 3 of 100 μl (MC25 + PBS).

5. Prepare membrane staining solution of mCLING, 0.1-0.2 μM in PBS. (about 0.15-0.50 μ g/ml) stock solution is 5 mg/ml.
6. Add the staining solution to each sample. Incubate for 15-30 mins at °C.
7. Centrifuge at 5000g for 1min and throw away supernatant. Add PBS.
8. Add IgG Xolair-AlexaFluor647 to 2 samples for each bacterial strain so that it has a concentration of 10 μ g/ml. The total sample volume should be 100 μl (50 AP1/MC25, 50 PBS, 1 (50mg/ml) IgG Xolair).
9. Incubate in dark for 30 minutes at 37°C on shake (300 rpm).
10. Fixate sample with ice cold 4% formaldehyde (1 ml of 16 % , 3 ml PBS) and 0.02% glutaraldehyde.
11. Place on ice for 10 mins. Work under hood with gloves!
12. Centrifuge samples at 5000g for 2 min and wash with PBS. Repeat once. For STED imaging, continue with step 12-15. For STORM imaging, continue with 16-19.
13. For STED imaging, apply 200 μl fibronectin solution of 5 mg/ml (stock solution diluted 1:200) on coverslips. Leave on overnight.
14. Throw away remaining liquid on the coverslip and add about 50 μl of the fixated samples. Leave on for 4 hours.
15. Apply 1 drop of ProLong gold antifade mountant on the specimen, carefully place the coverslip on the glass slide.
16. Let cure in the dark on flat surface (couple of hours to overnight)
17. For STORM imaging, apply 200 μ l of fibronectin solution of 5 mg/ml (stock solution diluted 1:200) on Matek dishes (No. 0). Leave on overnight.
18. Throw away remaining liquid on the Matek dishes and add about 50 μ l of the fixated sample Leave on for 4 hours.
19. Mix imaging buffer right before imaging session:

    Buffer reagents

    - 2-mercaptoethanol
    - 1M Tris (pH = 8.0)
    - Glucose Oxidase
    - COT (cyclooctatetraene)
    - Catalase from bovine - liver-lyophilized powder.

    Buffer solutions

    - Buffer A: 10 mM Tris + 50 nM NaCl
    - Buffer B: 50 mM Tris + 10 mM NaCl + 10 % Glucose
    - GLOX solution: 14 mg Glucose oxidase + 50 μ l Catalase (17mg/ml) + 200 μ l Buffer A. Vortex to dissolve glucose oxidase, spin down and use only supernatant.

Imaging buffer mix

- Combine 7 μl GLOX, 7 μl 2-mercaptoethanol, 7 μl COT and 690 μl Buffer B. Keep on ice.

A.2 Labelling mCLING with AlexaFluor594

This section describes the procedure for labelling membrane binding protein mCLING with maleimide activated AlexaFluor594 using the mCLING labelling kit from Synaptic Systems (710-MCK Synaptic Systems). The protocol follows manual from Synaptic Systems.

Solutions

- ALexaFluor594 maleimide
- DMSO
- Kit Content
  - Unlabelled mClING, 50nmol (lyophilized)
  - mCLING purification column
  - Washing Buffer, 10 ml
  - Stop solution, 0.5 ml
  - Elution buffer, 1ml
  - Neutralization Buffer, 0.5 ml

Labelling procedure

1. Dissolve mCLING with 100 μl deionized water (milliQ water) and transfer to eppendorf tube.
2. Dissolve maleimide activated AlexaFluor594 in DMSO to a concentration of 10 mg/ml.
3. Ad 100-200 nmol of AlexaFluor594 to the dissolved mCLING.
4. Incubate at room temperature rotating, for 2h.
5. Add 10 μl stopping solution and incubate for 20 min at room temperature.
6. Remove caps of the purification column and place in a 1,5 ml Eppendorf tube and let storage buffer drop out.
7. Transfer column to new 2 ml Eppendorf tube. Add 500 μl washing buffer and let drop out.
8. Transfer column to new 1.5 ml Eppendorf tube and apply labelling reaction to the column. Collect the flow through
9. Transfer column to new Eppendorf tube and add 500 μl washing buffer.

10. Transfer column to new Eppendorf tube and add 200 μl elution buffer. Collect the coloured eluate.
11. Add 20 μl of neutralization buffer and mix well.
12. Store labelled mCLING at -80 °Celsius.

B Julia-code for site localisation

```
#Code for producing intensity profiles of bacteria in two channel images and calculating
#the mean distance between the respective channel peaks.
#Load images and set variables to produce plots and distance calculation

#Importing necessary packages
using Images
using ImageFeatures
using ImageDraw
using CoordinateTransformations
using StaticArrays
using Plots
using Distributions
using ImageFiltering
using BioformatsLoader
using JavaCall
using StatsBase
using DSP
using Glob

gr() #set plotting backend

try
    JavaCall.init(["-ea", "-Xmx1024M", "-Djava.class.path=bioformats_package.jar"])
end


#Loading Images
image_dir = "../2018-02-28_Vibha_mCLING_Xolair/"
file_list = readdir(image_dir)
get_imgs = glob(image_dir * "2017-02-28_v*c*AUPH.msr")

#Set Variables
window = 5  #for sliding average, 0 if only aligning max of peaks
margin = 5  #how much to add on radius of fitted circle
radius_range = 25:40 #range in pixels of radius
PSF = 1.3 # sigma of PSF in pixels (Measured FWHM/2.3)
psf = Kernel.gaussian([PSF,PSF],[299,299]) #Creating gaussian kernel with sigma from measured FWHM
iterations = 100 # Deconvolution
threshold = 0.15 # To eliminate background inside cell
cutoff = 1
pixel_size = 15

max_radius = maximum(radius_range) + margin #Setting size for plots
allmemb = zeros(2*max_radius+1)
allantb = zeros(2*max_radius+1)
distance = Array{Array{Float64,1},1}()
n_theta = Array{Array{Int,1},1}()
```

```
#FUNCTIONS

# Add circle to image, adopted from ImageDraw (ellipse2d.jl)
function circle_add!(img::AbstractArray{T, 2}, center, radius) where T<:Integer
    ys = Int[]
    xs = Int[]
    cy, cx = center.I
    for i in cy : cy + radius
        for j in cx : cx + radius
            val = ((i - cy) / radius) ^ 2 + ((j - cx) / radius) ^ 2
            if val < 1
                push!(ys, i)
                push!(xs, j)
            end
        end
    end
    for (yi, xi) in zip(ys, xs)
        img[yi, xi] += 1
        if (yi != cy)
            img[2 * cy - yi, xi] += 1
        end
        if (xi != cx)
            img[yi, 2 * cx - xi] += 1
            if (yi != cy)
                img[2 * cy - yi, 2 * cx - xi] += 1
            end
        end
    end
    img
end

#Function for highpass-filtering images
function highpass(img, f)
    fftimg = fftshift(fft(ifftshift(gray.(img)), 1:2))
    sx, sy = size(fftimg)
    for x = 1:sx, y=1:sy
        if (x - sx/2.0)^2 + (y - sx/2.0)^2 < f^2
            fftimg[x,y] = 0
        end
    end
    return abs.(fftshift(ifft(ifftshift(fftimg))))
end

#Function for fitting circles using canny edge detector
function fit_circles(img)
    img_edge = canny(img,  (Percentile(99.0), Percentile(97.5)), 1.4)
    dx ,dy =imgradients(img, KernelFactors.ando5)
    img_phase = phase(dx,dy)
    centers, radii = hough_circle_gradient(img_edge, img_phase, 1, 35, 20, radius_range)
    return centers, radii, img_edge
end

#Function for finding circle on original image, polar transformed coordinates
function masked(img, center)
    mask = ((Polar(SVector(((i, j) .- center.I)...)), img[i,j]) for i=1:size(img, 1), j=1:size(img, 2))
    return mask
end

# Discretized polartransform
function polar_transform(masked, radius)
    circ = ceil(Int, 2*π*radius)
    polar_img = fill(-1., radius, circ)
```

```
    for (coord, val)=filter(x -> x[1].r < radius, masked)
        i = 1+floor(Int, coord.r)
        j = 1+floor(Int, (π+coord.θ)*radius)
        polar_img[i, j] = val
    end
    return polar_img
end

#Function for duplicating and filling in empty elements of polartransform
function duplicate_fill(polar_img)
    ind = indices(polar_img)
    polar_full = zeros(polar_img)
    circ = length(ind[2])
    for i = ind[1]
        for j = ind[2]
            nxt = 0
            val = -1.
            while val == -1.
                val = polar_img[i,1 + ((j+nxt+circ) % circ)]
                nxt = ~(nxt-signbit(nxt))
            end
            polar_full[i,j] = val
        end
    end
    return polar_full
end

# Function for Richardson Lucy Deconvolution
function rl_deconv(image::AbstractArray, psf::AbstractArray, iterations::Int)
    latent_est = Float64.(image)
    psf_hat = reflect(psf)
    interm = zeros(Float64, size(image))
    for i = 1:iterations
        # imfilter!(ArrayFireLibs(Algorithm.Mixed()), interm, latent_est, psf_hat)
        imfilter!(interm, latent_est, psf_hat)
        rel_blur = image ./ interm
        # imfilter!(ArrayFireLibs(Algorithm.Mixed()), interm, rel_blur, psf)
        imfilter!(interm, rel_blur, psf)
        latent_est .*= interm
    end
    return latent_est
end

# Function ensuring detected circles are in bounds
function circle_inbounds(center, radius, sz)
    for i=1:length(sz)
        if (center[i]-radius < 1) || (center[i]+radius > sz[i])
            return false
        end
    end
    return true
end

for file_index = 1:Int(length(get_imgs))

    #Importing images
    fname = get_imgs[file_index]
    channels = @. bf_import(image_dir * fname, stdout_redirect=DevNull)
    antibodies = data(channels[2])
    membrane  = data(channels[1])

    #Deconvolving images
```

```
membrane = rl_deconv(membrane, psf, iterations)
antibodies = rl_deconv(antibodies, psf, iterations)

#Normalizing images
my_norm(image) = (e -> (image-e[1]+eps()).*(1/(e[2]+eps()-e[1])))(extrema(image))
antibodies = my_norm(antibodies)
membrane = my_norm(membrane)
#save("deconv.png", antibodies)

#implementing fit_circles on membrane channel
centers, radii, membraneEdge = fit_circles(membrane)

# Check if circles are in bound
circles = filter(x -> circle_inbounds(x[1], x[2]+margin, size(membrane)), zip(centers, radii))
centers2, radii2, antibodyEdge = fit_circles(antibodies)

#Drawing circles on membrane Image
membraneEdge = Gray.(membraneEdge)
for (center, radius) in circles
    #println("$center $radius $(size(membrane)) $(circle_inbounds(center,radius,size(membrane)))")
    draw!(membraneEdge, CirclePointRadius(center, radius))
end

#Save Images
save("membrane_edge.png", membraneEdge)
save("membrane_norm.png", membrane)
save("antibody_edge.png", antibodyEdge)

# circle fill: on zero matrix += ones for each circle, to localize overlap
circle_img = zeros(Int,size(membrane))
for (center, radius) in circles
    try
        circle_add!(circle_img, center, radius+margin)
    end
end
save("tmp.png", Gray.(float(circle_img)/maximum(circle_img)))

# Find all elements in circle_img > 1 (the elements with overlap)
list_overlap = find(x -> x > 1, circle_img)
list_overlap = ind2sub(circle_img, list_overlap)

# Find elements in circle
in_circle(c, r, x, y) = ((x-c[1])^2 + (y-c[2])^2) <= r^2

#Define totalmemb and totalantb
totalmemb = zeros(2*max_radius+1)
totalantb = zeros(2*max_radius+1)

#Define sumdistance, n, n_theta, and distance to calculate average distance
#and weighted standard deviation
sumdistance = zeros(1)
n = zeros(1)
push!(distance, Array{Float64,1}())
push!(n_theta, Array{Int,1}())

#Polartransform and alignment of intensity profiles in each detected circle
#Implementing on both image channels
for (center, radius) in circles

    #Adding margin to detected circle to include more information in the
    #intensity profile, defining circumference
    radius += margin
```

```
circ = ceil(Int, 2*π*radius)

#Loacalizing circles in the original image, creating masks
memb_masked = masked(membrane, center)
antb_masked = masked(antibodies, center)

#Polartransforming masks
memb_polar_img = polar_transform(memb_masked, radius)
memb_polar_full = duplicate_fill(memb_polar_img)
antb_polar_img = polar_transform(antb_masked, radius)
antb_polar_full = duplicate_fill(antb_polar_img)
save("memb_polar_full.png", memb_polar_full)
save("antb_polar_full.png", antb_polar_full)

#Listing theta of intensity profiles with overlap
overlap = filter(t -> in_circle(center, radius, t[1], t[2]), zip(list_overlap...))
polar_overlap = (Polar(SVector(t .- center.I)) for t=overlap)
discrete_theta = Set(1+floor(Int, (π+c.θ)*radius) for c=polar_overlap)

# for subtract inner intensity
#memb_polar_full .-= mean(memb_polar_full[1:cutoff,:])
#antb_polar_full .-= mean(antb_polar_full[1:cutoff,:])
#memb_polar_full = clamp01.(memb_polar_full)
#antb_polar_full = clamp01.(antb_polar_full)


# for elimintating intenisty inside cell
#thresh = threshold*maximum(memb_polar_full)
#memb_polar_full = memb_polar_full[cutoff:radius, :]
#antb_polar_full = antb_polar_full[cutoff:radius, :]
#antb_polar_full = find( antb_polar_full.>threshold*maximum(antb_polar_img))
#radius = size(memb_polar_full, 1)

#Fit gaussian to each intensity profile
n_radius = zeros(radius*2+1)
r = 1:radius
dist_fitting = mapslices(x-> fit_mle(Normal, r , x), memb_polar_full[cutoff:radius, :], (1))
maxPeaks = round(Int, mean.(dist_fitting))

#Alternative: Sliding average to find max peak of each intensity profile
#movmax(v) = window + indmax(mean(v[i-window:i+window]) for i=1+window:length(v)-window)
#maxPeaks = mapslices(movmax, memb_polar_full, (1))

#Define memb_shift and antb_shift for alignment
memb_shift = zeros(2*radius+1)
antb_shift = zeros(2*radius+1)

#Performing alignment and excluding overlap
for θ = 1:circ
    if !in(θ, discrete_theta)

        shift_ind = (1:radius) + radius + 1 - maxPeaks[θ]
        memb_shift[shift_ind] += memb_polar_full[:,θ]
        antb_shift[shift_ind] += antb_polar_full[:,θ]
        n_radius[shift_ind] += 1
    end

end

#Plotting sumed radial intensity of each fitted circle, both channels
#plot(1:radius, memb_polar_img./n_radius, label="Membrane")
#plot(-radius:radius, antb_shift/circ, label="Antibody")
```

```
        #plot!(-radius:radius, memb_shift/circ, label="Membrane")
        #savefig("artifacts/plot$k.png")

        #Normalizing and summing up intensity profiels from each mask
        range_total = (-radius:radius) + 1 + max_radius
        totalantb[range_total] += antb_shift./n_radius
        totalmemb[range_total] += memb_shift./n_radius

        # Fit gaussians to membrane channel for each mask for calculating distance
        rad = collect(-radius:radius)
        dist_fittingmemb = fit_mle(Normal,rad ,  memb_shift)
        #Extract mean of gaussian
        maxPeaksmemb = round(Int, mean.(dist_fittingmemb))

        # Fit gaussians to antbpolarfull for calculating distance
        dist_fittingantb = fit_mle(Normal, rad,  antb_shift)
        #Extract mean of gaussian
        maxPeaksantb = round(Int, mean.(dist_fittingantb))

        # Calculating distances
        append!(distance[end], maxPeaksantb - maxPeaksmemb)
        append!(n_theta[end], circ - length(discrete_theta))
    end

    #Plot of intensity profile of each image
    plot(-max_radius:max_radius, totalmemb, label="Antibody")
    plot!(-max_radius:max_radius, totalantb, label="Membrane")

    savefig("artifacts/tot$file_index.png")

    #Summing all images
    allantb += totalantb
    allmemb += totalmemb
end

#For plotting allmemb and allantb intensity profiles
begin notnan(x) = ~isnan(x)
    antb_max = maximum(filter(notnan, allantb))
    memb_max = maximum(filter(notnan, allmemb))
    first = findfirst(notnan, allmemb)
    last = findlast(notnan, allmemb)
    plotrange = (0:(last - first))*pixel_size
    #Plots.scalefontsizes(1.2)
    plot(plotrange, allmemb[first:last]./memb_max, label="Antibody", linewidth = 2,
    linecolor = :red, legend = :bottomleft)
    plot!(plotrange, allantb[first:last]./antb_max, label="Membrane",
    linewidth = 2, linecolor = :green, legend = :bottomleft)
    xlabel!("radius (nm)")
    ylabel!("Intensity")
    savefig("artifacts/sumofall.png")
end

#To calculate average distance between peaks, confidence interval,
#weighted standard deviation and perform t-test for t = 2.26 (alpha = 0.05)
distance_all = [d for arr in distance for d in arr]
n_theta_all = [n for arr in n_theta for n in arr]

function stats(distance, n_theta)
    n = length(distance)
    avgdistance = sum(distance.*n_theta)./sum(n_theta)
    stdev = std(distance, weights(n_theta), corrected=false)
    t0 = avgdistance/(stdev./(n).^0.5)
```

```
    conf_int = t*stdev/n^0.5
    return avgdistance, stdev, n, t0, conf_int
end

t = 2.262;
avgdistance, stdev, n, t0, conf_int = stats(distance_all, n_theta_all)
println("avg:$avgdistance, std:$stdev, n:$n, t0:$t0, conf_int:$conf_int")

#List results from each image, to identify potential outliers.
open("results.csv","w") do f
    for i=1:length(distance)
        avgdistance, stdev, n, t0, conf_int = -1, -1, -1, -1, -1
        try
            avgdistance, stdev, n, t0, conf_int = stats(distance[i], n_theta[i])
        end
        write(f, "$i, $(get_imgs[i]), avg:$avgdistance, std:$stdev, n:$n, t0:$t0, conf_int:$conf_int\n")
    end
end
```